RSC Advances

PAPER

View Article Online
View Journal | View Issue

Cite this: *RSC Adv.*, 2021, **11**, 7886

Enhanced high voltage performance of $LiNi_{0.5}Mn_{0.3}Co_{0.2}O_2$ cathode *via* the synergistic effect of $LiPO_2F_2$ and FEC in fluorinated electrolyte for lithium-ion batteries

Rui Li,[a] Pan Zhang,[a] Jian Huang,[a] Boyu Liu,[a] Mingjiong Zhou, *[a] Bizheng Wen,*[b] Yu Luo[c] and Shigeto Okada[d]

$LiNi_{0.5}Mn_{0.3}Co_{0.2}O_2$ can achieve high energy density due to its merits of high theoretical capacity and a relatively high operating voltage, but the $LiNi_{0.5}Mn_{0.3}Co_{0.2}O_2$ battery suffers from capacity decay because of the unstable solid electrolyte interface on the cathode. Herein, we investigate the application of a fluorinated electrolyte composed of fluoroethylene carbonate (FEC) as a cosolvent and lithium difluorophosphate ($LiPO_2F_2$) as a salt-type additive extending the life span of the $LiNi_{0.5}Mn_{0.3}Co_{0.2}O_2$ cathode. $LiNi_{0.5}Mn_{0.3}Co_{0.2}O_2$ can achieve and maintain a capacity of 157.7 mA h g^{-1} over 200 cycles at a 1C rate between 3.0 and 4.4 V, as well as a reversible capacity of 132.7 mA h g^{-1} even at the high rate of 10C. The enhanced performance can be ascribed to the formation of the robust and protective fluorinated organic–inorganic film on the cathode, which derives from the FEC cosolvent and $LiPO_2F_2$ additive and ensures facile lithium-ion transport. The synergistic effect of the cosolvent and additive to boost the electrochemical performance of $LiNi_{0.5}Mn_{0.3}Co_{0.2}O_2$ cathode will pave a new pathway for high-voltage cathode materials.

Received 6th December 2020
Accepted 3rd February 2021

DOI: 10.1039/d0ra10280f

rsc.li/rsc-advances

1. Introduction

Lithium-ion batteries (LIBs) have been perceived as suitable power sources for portable electronic devices and have emerged remarkably in our daily lives.[1] Cathode materials that operate at high voltages have been developed to increase the energy density of LIBs.[2–4] However, the overcharged cathode also accelerates the decomposition of the electrolytes at high potential,[5,6] resulting in the formation of an unstable solid electrolyte interphase (SEI) film composed of organic carbonate and inorganic lithium salts on the cathode surface.[7,8] It is well known that the conventional organic electrolyte results in a poor and thick SEI layer, which contains a large number of the resistive decomposition products of LiF and Li_2CO_3,[9] as well as other inorganic and organic by-products.[10] To achieve the high energy density, LIBs are operated at high voltage accompanied by the decomposition of the electrolyte[11–14] and the collapse of the structure of the electrode,[13,15] which ultimately leads to poor electrochemical performance. Therefore, new electrolyte components, especially solvents and additives, must be developed to accommodate those high-potential applications.

Recently, fluorinated SEI film generated by the decomposition of fluorinated solvents or anions was reported as a stable film that can regulate the diffusion behavior of lithium ions and extend the life of LIBs.[16,17] A fluoroethylene carbonate (FEC) has been developed to effectively improve the electrochemical performances and change the nature of the SEI layer of electrodes in LIBs.[18] Aurbach *et al.* demonstrated the excellent cycling stability of Li|Li symmetric cells and Li|NCM cells in the FEC-based electrolyte, because of the formation of a stable SEI on the electrode surface.[19,20] Replacing EC with FEC in the electrolyte for high-voltage LIBs showed dramatically improved cycling behavior of $LiCoPO_4$/Li cells due to the formation of an effective protective film on the cathode.[21] Sun *et al.* reported that the prominent cycling stability and high coulombic efficiency under the high areal loading conditions of $LiNi_{0.6}Mn_{0.2}Co_{0.2}O_2$/Li batteries were achieved by combining traditional ethyl methyl carbonate (EMC) with FEC solvents.[10] Cryo-electron microscopy as a powerful analytical technique was used to reveal the nanostructure of SEI influenced by FEC; unlike a mosaic film in an electrolyte without FEC, the SEI formed in the FEC-containing electrolyte was a multilayer nanostructure film.[22,23]

[a]*School of Materials Science and Chemical Engineering, Ningbo University, Fenghua Road 818, Jiangbei District, Ningbo 315211, Zhejiang Province, People's Republic of China. E-mail: zhoumingjiong@nbu.edu.cn*

[b]*Ningbo Procutivity Promotion Center, Yangfan Road 999, Hi-tech Zone, Ningbo 315100, Zhejiang Province, People's Republic of China*

[c]*Ningbo Nanomicro Energy Technology Co., Ltd., Ningbo 315800, Zhejiang Province, People's Republic of China*

[d]*Institute for Materials Chemistry and Engineering, Kyushu University, 6-1 Kasuga-koen, Kasuga 816-, 8580, Japan*

The resultant SEI interface generated from the organic film-forming electrolyte is less ionically conductive than those generated from the decomposition of inorganic salt. Lithium difluorophosphate ($LiPO_2F_2$) as a new salt-type additive has attracted a lot of attention and participated in the formation of a film on graphite with high ionic conductivity and stable surface to enhance the high rate performance of graphite electrodes.[24,25] $LiPO_2F_2$ can also improve the performance of LIBs under high voltages due to a stable SEI film formed on the cathode surface.[26–28] The stable SEI film can effectively prevent direct contact between the cathode material and the electrolyte, thus suppressing the detrimental interfacial reactions. Even though $LiPO_2F_2$ has been reported before, it is usually studied alone, or in combination with other additives. The cooperation of the organic cosolvent and inorganic additive in an electrolyte has multiple benefits that can play a synergistic role, neutralize their drawbacks and improve the comprehensive performance of LIBs. The resultant organic–inorganic SEI film derived from organic cosolvent and inorganic lithium salts exhibits high ionic conductivity, which not only decreases the interfacial resistance, it also enhances the stability of the electrode/electrolyte interface, resulting in the suppression of the oxidation of the electrolyte and the dissolution of transition metal ions. To the best of our knowledge, the effectiveness of $LiPO_2F_2$ in an EC-free FEC-based electrolyte has not been reported for high-voltage LIBs. In this work, $LiPO_2F_2$ as an additive was applied in 1 M $LiPF_6$/FEC/DMC solution for LIBs. The electrochemical performance of the $LiNi_{0.5}Mn_{0.3}Co_{0.2}O_2$ cathode in a $LiPO_2F_2$-containing FEC-based electrolyte was investigated and the effect of the $LiPO_2F_2$-containing FEC-based electrolyte was clarified under high voltage.

2. Experimental

The EC-based electrolyte consists of 1.0 M $LiPF_6$ in the solvent mixture of ethylene carbonate (EC) and dimethyl carbonate (DMC) (3 : 7 by volume). The FEC-based electrolyte was prepared by dissolving 1.0 M $LiPF_6$ in a solvent mixture of fluoroethylene carbonate (FEC) (98%, Macklin Co., Ltd.) and DMC (3 : 7 by volume) in the glove box filled with Ar gas. Hybrid electrolytes were prepared by the addition of 1 wt% $LiPO_2F_2$ (Ningbo Nanomicro Energy Technology Co., Ltd.) to the FEC-based electrolyte. The viscosities and conductivities of the

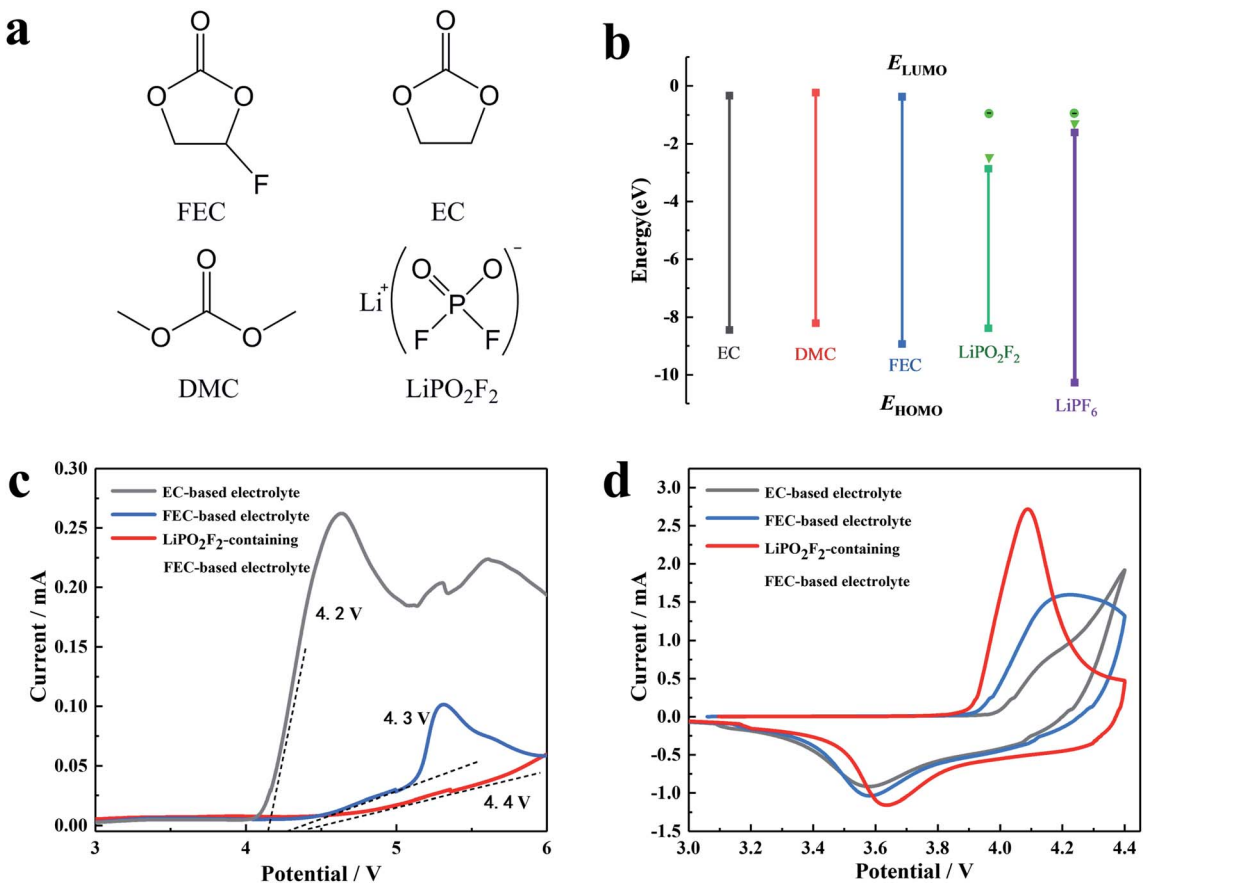

Fig. 1 (a) Molecular structure of the electrolyte components (FEC, EC, $LiPO_2F_2$, and DMC). (b) The HOMO/LUMO energies of the various components in the electrolyte. (c) LSV curves of the electrolyte solution: EC-based electrolyte (1 M $LiPF_6$/EC + DMC), FEC-based electrolyte (1 M $LiPF_6$/FEC + DMC) and $LiPO_2F_2$-containing FEC-based electrolyte (1 M $LiPF_6$/FEC + DMC with 1 wt% $LiPO_2F_2$) in the potential range of 3.0–6.0 V at a scan rate of 5 mV s^{-1}. (d) Cyclic voltammogram of $LiNi_{0.5}Mn_{0.3}Co_{0.2}O_2$ cathodes with various electrolytes between 3.0 and 4.4 V at a scan rate of 1 mV s^{-1}.

electrolyte were measured by a DV-2T viscometer (Brookfield, USA) and FE38 standard conductivity meter (Mettler-Toledo, Switzerland) at temperatures ranging from 298 K to 338 K. The color changes and acidities of the samples before and after storage were monitored by photographs and pH paper (Sinopharm Chemical Reagent Co. Ltd.), respectively. The solvent molecules (EC, FEC and DMC), lithium salt ($LiPF_6$) and additive ($LiPO_2F_2$) in the electrolyte were geometrically optimized and the relative energy calculated using the Gaussian 09 software. In addition, the B3LYP density functional theory with 6-311+G(d, p) basis set was used to calculate the highest unoccupied molecular orbital energy and the lowest unoccupied molecular orbital energy (E_{HOMO} and E_{LUMO}).

Slurries were prepared containing 80 wt% active materials, 10 wt% super P and 10 wt% PVdF in *N*-methyl-2-pyrrolidone. The slurries were coated onto aluminum foil and dried at 110 °C for 12 h in a vacuum oven, and then punched into 12 mm diameter disks for testing. The electrochemical properties were investigated using CR2032 coin-type half-cells, which were assembled in a glove-box filled with argon. A lithium-foil and a polypropylene film (Celgard 3501) were used as the counter electrode and separator, respectively. The galvanostatic charge/discharge tests were carried out at a constant current density between 3.0 and 4.4 V using a LAND battery system (Wuhan, China). The electrochemical window of electrolytes was studied by linear sweep voltammetry (LSV) between 3.0 and 6.0 V *vs.* Li/Li^+ with a scan rate of 5 mV s^{-1}. Cyclic voltammetry (CV) measurements were performed in the potential range of 3.0–4.4 V at a scan rate of 1 mV s^{-1}. Electrochemical impedance spectroscopy (EIS) studies were conducted using an AC amplitude of 5 mV in a frequency range of 0.01–100 kHz. LSV, CV and EIS tests were collected by a CHI-660E workstation at 25 °C. LSV was taken on stainless steel/Li cells, while the $LiNi_{0.5}Mn_{0.3}Co_{0.2}O_2$/Li cells were used for CV and EIS tests.

To analyze the surface component and morphology of the $LiNi_{0.5}Mn_{0.3}Co_{0.2}O_2$ cathodes, the cells before and after cycling were disassembled in a glove box. The electrodes were soaked in DMC for 1 h to remove the residual electrolyte, and dried under vacuum at room temperature. The morphology of the electrodes was observed by scanning electron microscopy (SEM, Hitachi, Japan) and transmission electron microscopy (TEM, Tecnai F30, Netherlands). The chemical analysis of surface compositions was characterized by X-ray photoelectron spectroscopy (XPS, Thermo Scientific K-Alpha).

3. Results and discussion

The chemical structure and molecular orbital energies of the electrolyte components, as well as the electrochemical stabilities of the electrolytes are shown in Fig. 1. Fig. 1a and b show the chemical structure of the electrolyte components, the highest

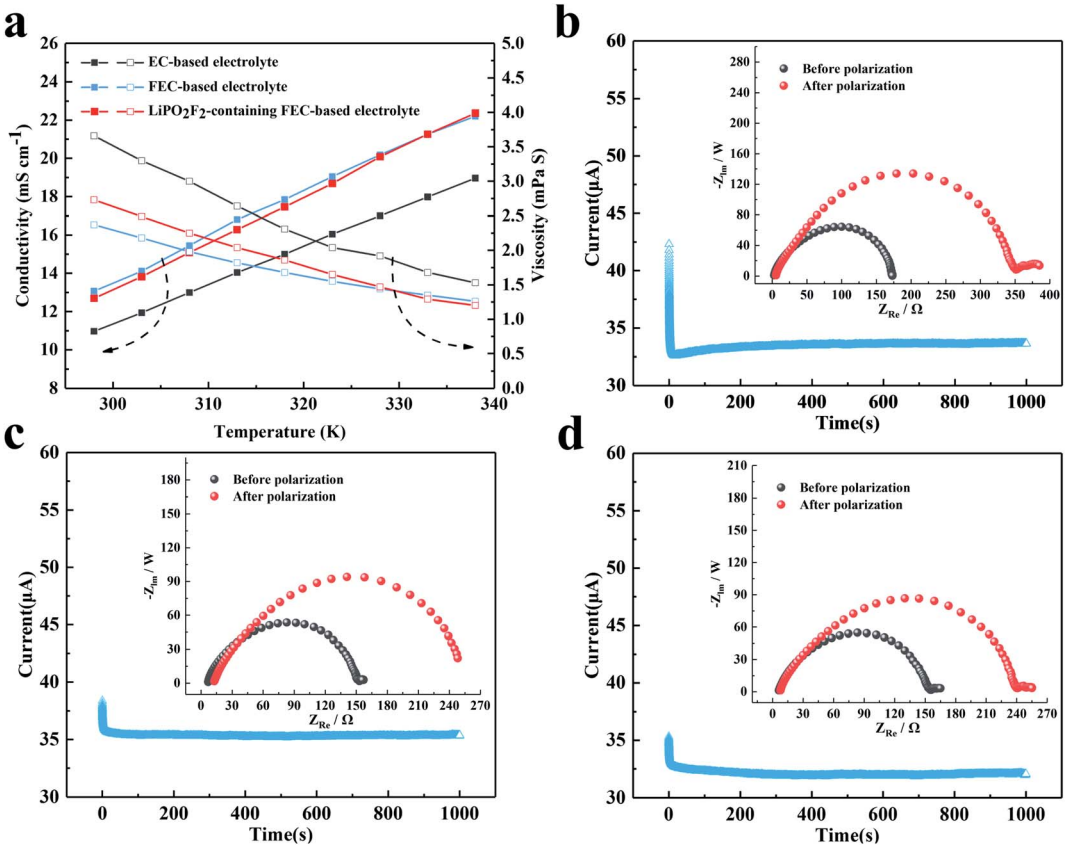

Fig. 2 (a) Conductivity and viscosity of the electrolyte solution: EC-based electrolyte, FEC-based electrolyte and $LiPO_2F_2$-containing FEC-based electrolyte. Chronopotentiometry for (b) EC-based electrolyte, (c) FEC-based electrolyte, and (d) $LiPO_2F_2$-containing FEC-based electrolyte.

occupied molecular orbital (HOMO) energies, and the lowest unoccupied molecular orbital (LUMO) energies, respectively. For the molecule with higher HOMO energy, the electron in the outermost layer has higher energy and tends to be lost more easily at high voltage, resulting in the oxidization of the molecule at a lower voltage. It was found that FEC has lower HOMO energy than other solvents (EC and DMC). Hence, the FEC replacing the EC as the cosolvent in the electrolyte can broaden the electrochemical window. For the molecule with a lower LUMO energy, the foreign electrons are more likely to occupy this orbital, and thus the molecule is reduced at a higher voltage. It can be seen that $LiPO_2F_2$ had a lower LUMO energy, reflecting stronger electron affinity.

The electrochemical stabilities of the electrolytes were investigated by linear sweep voltammetry (LSV), as shown in Fig. 1c. The oxidation current of the cosolvent EC-based electrolyte appeared at around 4.1 V (*vs.* Li/Li^+) and increased above 4.2 V (*vs.* Li/Li^+), while the decomposition voltage of the FEC-based electrolyte was around 4.3 V (*vs.* Li/Li^+). After the addition of $LiPO_2F_2$ to the FEC-based electrolyte, the starting oxidation potential of the FEC-based electrolyte increased to approximately 4.4 V (*vs.* Li/Li^+). Furthermore, the oxidation current of the $LiPO_2F_2$-containing FEC-based electrolyte was relatively small and remained stable in the voltage range of 4.3–6.0 V, suggesting that the combination of the FEC cosolvent and the $LiPO_2F_2$ additive can increase the anodic limiting potential.

Table 1 The values of the parameters used to determine the lithium transference numbers (t_{Li^+}) in eqn (1) at 25 °C

Sample	I_0 (μA)	I_{SS} (μA)	R_0 (Ω)	R_{SS} (Ω)	ΔV (mV)	t_{Li^+}
EC-based electrolyte	42.32	33.56	173.9	358.8	10	0.48
FEC-based electrolyte	38.37	35.34	148.2	262.2	10	0.56
$LiPO_2F_2$-containing FEC-based electrolyte	35.32	32.03	150.1	240.2	10	0.62

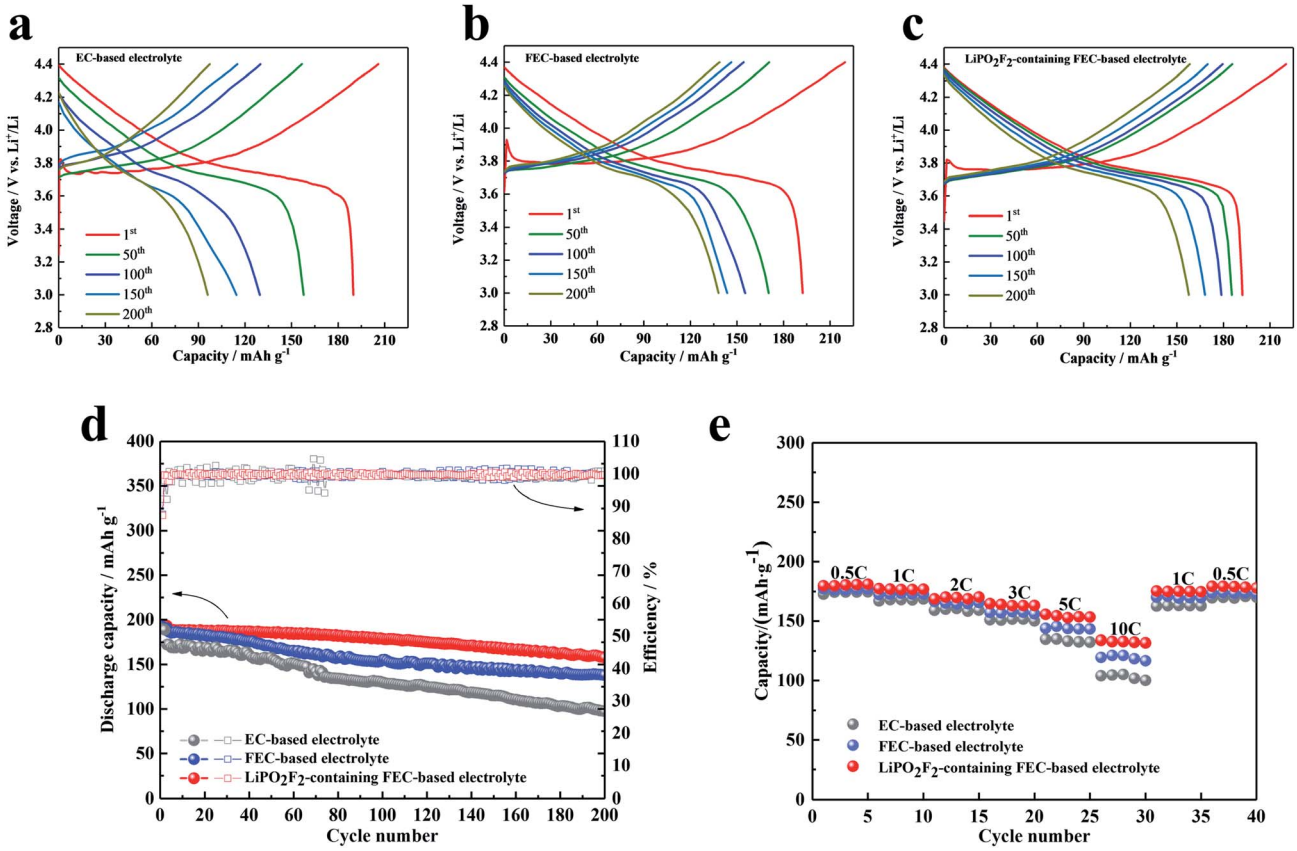

Fig. 3 Charge/discharge curves of $LiNi_{0.5}Mn_{0.3}Co_{0.2}O_2$ cathodes with the (a) EC-based electrolyte, (b) FEC-based electrolyte, and (c) $LiPO_2F_2$-containing the FEC-based electrolyte at voltages ranging from 3.0 to 4.4 V. (d) Cycling performances and coulombic efficiencies of $LiNi_{0.5}Mn_{0.3}Co_{0.2}O_2$ cathodes with various electrolytes between 3.0 and 4.4 V. (e) Rate capability of $LiNi_{0.5}Mn_{0.3}Co_{0.2}O_2$ cathodes in various electrolytes.

Fig. 1d shows the CV curves of the first cycle of the $LiNi_{0.5}Mn_{0.3}Co_{0.2}O_2$ cathode in various electrolytes. A pair of oxidation/reduction peaks accompanied by Ni^{2+}/Ni^{4+} and Co^{3+}/Co^{4+} were observed during the Li^+ extraction and insertion.[29,30] Among them, the oxidation and reduction peaks of the FEC-based electrolyte containing $LiPO_2F_2$ were more obvious and the distance between these two peaks was closer. These results indicated that the FEC cosolvent and $LiPO_2F_2$ additive can significantly alleviate the electrochemical polarization, and the Li^+ insertion/extraction process became much more reversible.

The conductivity and viscosity of the electrolyte play an important role in the performance of a battery. Fig. 2 shows the conductivity, viscosity and lithium-ion transference number of the electrolytes. As shown in Fig. 2a, the FEC-based electrolytes exhibited higher conductivity and lower viscosity than the EC-based electrolyte. However, the addition of 1 wt% $LiPO_2F_2$ to the FEC-based electrolyte resulted in a slight decrease in the conductivity and an increase in the viscosity, due to the dissociation energy of $LiPO_2F_2$ being higher than that of $LiPF_6$. Fig. 2b–d show the dc polarization current responses, and the corresponding impedance spectra before and after the dc polarization of the Li/Li symmetric cells. The Li^+ migrations were calculated according to eqn (1),[31–35] and are summarized in Table 1:

$$t_{Li^+} = \frac{I_s(\Delta V - I_0R_0)}{I_0(\Delta V - I_sR_s)} \quad (1)$$

I_o and I_s are the initial state and steady-state currents. R_o and R_s are the initial resistance and stable resistance of the passivation layer, respectively. ΔV is the voltage applied across the Li/Li cell. The EIS measurements of the symmetric cell were carried out before and after polarization, and an interval of an hour between the tests was needed to reach a quasi-equilibrium state. The polarization measurements were applied a 10 mV dc voltage to a symmetrical battery, and a stable current was obtained after 1000 s. The respective values of t_{Li^+} for the EC-based electrolyte, FEC-based electrolyte and $LiPO_2F_2$-containing FEC-based electrolyte at 25 °C were 0.48, 0.56 and 0.62, respectively. It was demonstrated that the O^{2-} electron cloud of $LiPO_2F_2$ had a strong attraction to Li^+ and caused anion deformation due to the strong anion coordination effect.[26] Hence, this effect enhanced the dissociation effect of the Li^+ and PF_6^- ion-pair, and then made Li^+ easier to move in the electrolyte, resulting in a high lithium-ion transference number (t_{Li^+}).[36]

Fig. 3 shows the electrochemical properties of $Li/LiNi_{0.5}Mn_{0.3}Co_{0.2}O_2$ cells cycled in different electrolytes between 3.0 and 4.4 V at 1C rate (three activated cycles with 0.1C rate). Fig. 3a–c present the voltage profiles of the $Li/LiNi_{0.5}Mn_{0.3}Co_{0.2}O_2$ cell in various electrolytes for the 1st, 50th, 100th, 150th and 200th cycles, respectively. The initial charge and discharge capacities of the cell with the EC-based electrolyte were 205.9 mA h g^{-1} and 189.9 mA h g^{-1}, respectively, which corresponded to an initial coulombic efficiency of 92.2%. The cell cycled in FEC-based electrolyte without additive exhibited

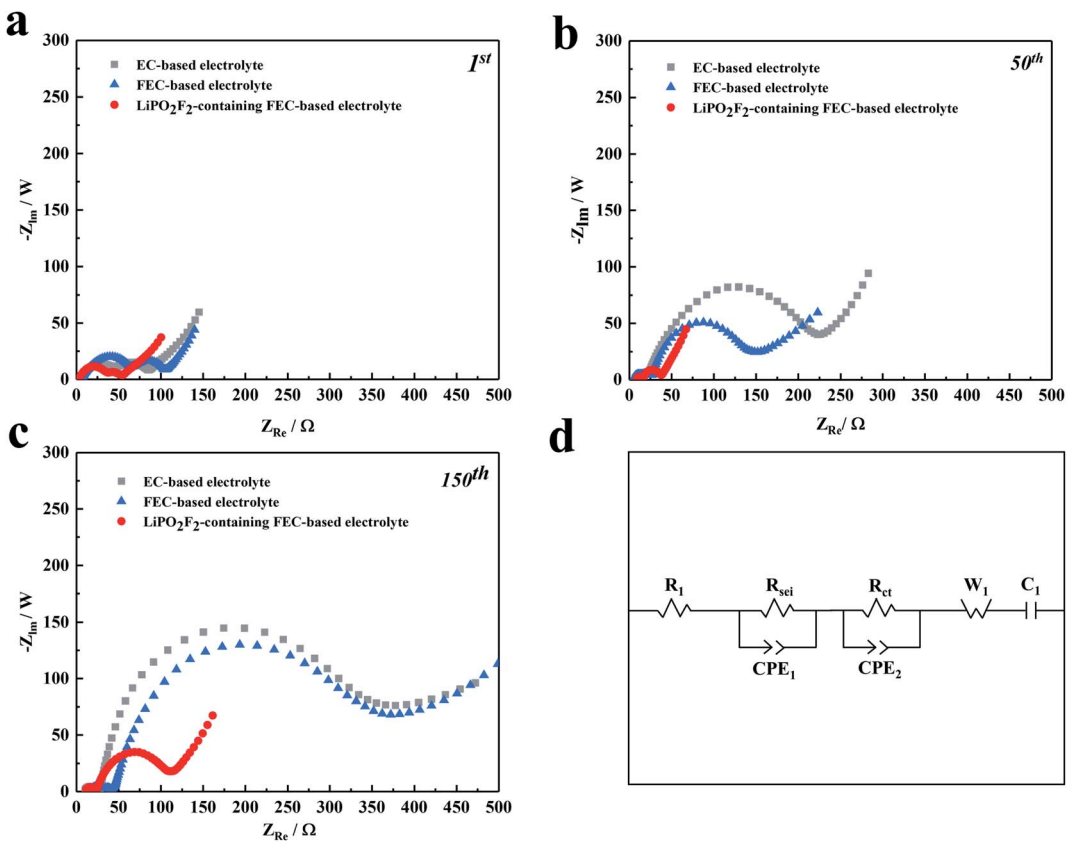

Fig. 4 Nyquist plots of $LiNi_{0.5}Mn_{0.3}Co_{0.2}O_2/Li$ cells in various electrolytes: (a) after 1 cycle, (b) after 50 cycles, and (c) after 150 cycles, respectively. (d) The corresponding equivalent circuit model.

Table 2 Fitted data for the EIS spectra of $LiNi_{0.5}Mn_{0.3}Co_{0.2}O_2$ cells with various electrolytes

	After 1 cycle		After 50 cycles		After 150 cycles	
Sample	R_{sei} (Ω)	R_{ct} (Ω)	R_{sei} (Ω)	R_{ct} (Ω)	R_{sei} (Ω)	R_{ct} (Ω)
EC-based electrolyte	67.24	57.64	29.26	219	33.78	330.1
FEC-based electrolyte	44.35	55.32	10.4	125.5	14.8	325.3
$LiPO_2F_2$-containing FEC-based electrolyte	35.33	26.78	7.25	22.74	11.51	90.1

a lower initial coulombic efficiency of 87.5% (discharge and charge capacities were 192.3 mA h g^{-1} and 219.6 mA h g^{-1}, respectively). Similar to the FEC-based electrolyte, the cell cycled with the $LiPO_2F_2$-containing FEC-based electrolyte also showed a coulombic efficiency of 87.2%. This low initial coulombic efficiency was attributed to the electrolyte decomposition with the formation of the SEI film on the cathode. After the second cycle, the charge and discharge process proceeded reversibly, although the capacity generally decreased for all samples. Fig. 3d compares the cyclic stability of batteries with various electrolytes at 1C rate (three activated cycles with 0.1C rate). It can be seen that the cells in the FEC-based electrolyte showed better cyclic stability than that in the EC-based electrolyte, due to a more stable SEI film formed in the FEC-based electrolyte.[19] Furthermore, with the addition of $LiPO_2F_2$ in the FEC-based electrolyte, the cyclic stability was remarkably improved, and the capacity decreased from 192.2 mA h g^{-1} to 157.7 mA h g^{-1} for up to 200 cycles, corresponding to a capacity retention of 82.1%. This phenomenon can be attributed to an excellent film on the cathode surface modified by the $LiPO_2F_2$, which can suppress the further decomposition of the solvents, resulting in enhanced interfacial stability of the cathode/electrolyte and the cyclic stability of the $LiNi_{0.5}Mn_{0.3}Co_{0.2}O_2$ cathode.[26–28]

The rate capability of the $LiNi_{0.5}Mn_{0.3}Co_{0.2}O_2$ cells with various electrolytes was also compared. Fig. 3e shows the specific capacities of the $LiNi_{0.5}Mn_{0.3}Co_{0.2}O_2$ cathode at current densities of 0.5C, 1C, 2C, 3C, 5C, and 10C (1C = 170 mA h g^{-1}) in the voltage range of 3.0–4.4 V. Because of the higher lithium-ion transference number, the FEC-based electrolytes exhibited a better rate performance than the EC-based electrolyte. Moreover, the battery with the $LiPO_2F_2$-containing FEC-based electrolyte can reach a specific capacity of 132.7 mA h g^{-1}, even at the high rate of 10C. This observation added evidence for the extremely stable SEI film formed on the cathode surface with high ionic conductivity, accompanied by the electrochemical decomposition of the FEC cosolvent and $LiPO_2F_2$ additive.

The synergistic effectiveness of $LiPO_2F_2$ and FEC in the fluorinated electrolyte on the performance of $LiNi_{0.5}Mn_{0.3}Co_{0.2}O_2$ cells was further investigated by EIS measurements. Fig. 4 shows Nyquist plots for the $LiNi_{0.5}Mn_{0.3}Co_{0.2}O_2$ cells before and after 1, 50, and 150 cycles, respectively, together with

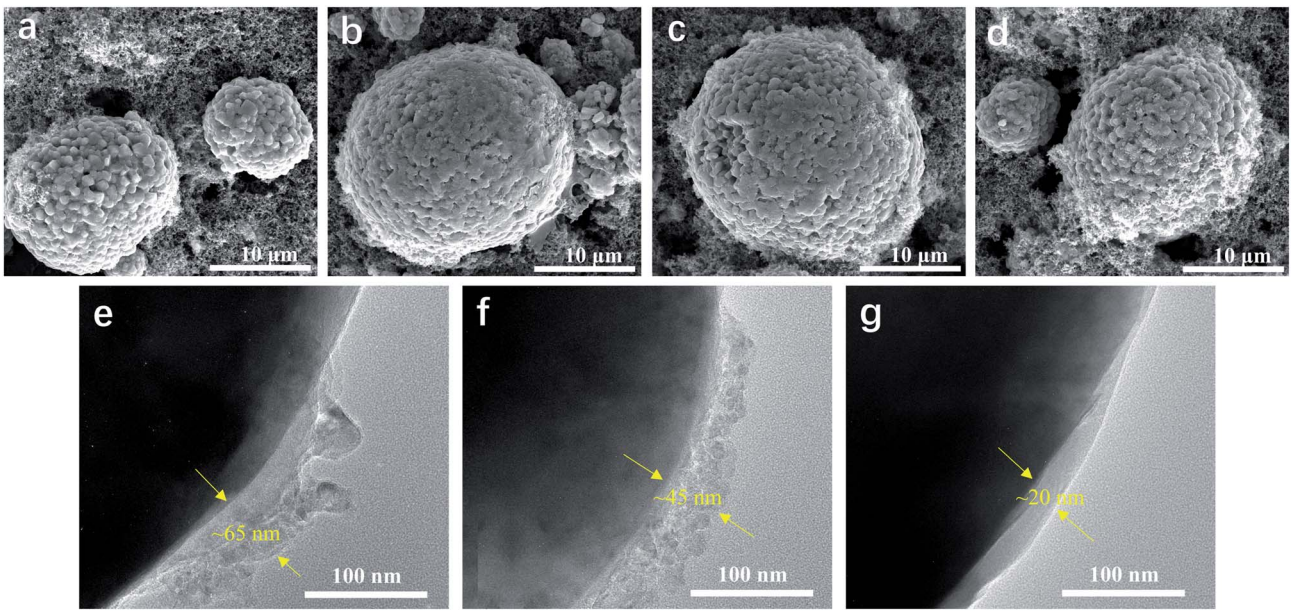

Fig. 5 SEM images of (a) pristine and cycled $LiNi_{0.5}Mn_{0.3}Co_{0.2}O_2$ electrodes with (b) the EC-based electrolyte, (c) FEC-based electrolyte, and (d) $LiPO_2F_2$-containing the FEC-based electrolyte after 100 cycles. TEM images of cycled cathodes with (e) the EC-based electrolyte, (f) FEC-based electrolyte, and (g) $LiPO_2F_2$-containing FEC-based electrolyte after 100 cycles.

the corresponding equivalent circuit model. The values of interface resistance and electrolyte resistance estimated from the impedance spectra are illustrated in Table 2. All the EIS spectra consist of two semicircles in the high-medium frequency region and a sloped line in the low-frequency region. The high-frequency semicircle is associated with the electrode surface film resistance (R_{sei}), while the mid-frequency semicircle represents the charge transfer resistance (R_{ct}) between the electrodes. The straight line in the low-frequency region is ascribed to the Warburg impedance (W_1, relating to Li^+ diffusion within the electrode).[37–39] It was noted that the semicircles of samples increased continuously with cycling at high-medium frequency, which was ascribed to the progressive growth of SEI on the cathode surface and the increased thickness of the SEI film caused by the electrolyte decomposition. Both resistances, R_{sei} and R_{ct}, increased from the 1st to the 150th cycle in the following order: $LiPO_2F_2$-containing FEC-based electrolyte < FEC-based electrolyte < EC-based electrolyte. It was implied that the surface film formed on the cathode in the EC-based solution was thicker than that in the FEC-based solution. The replacement of EC by FEC could change the composition of the SEI film, making it easier for Li^+ to pass through the interface layer.[19] More importantly, the increase in R_{ct} slowed down significantly with cycling for cells after the addition of $LiPO_2F_2$ in the electrolyte, which confirmed that a relatively stable SEI film was formed on the cathode surface by the FEC cosolvent and $LiPO_2F_2$ additive, resulting in the mitigation of the internal impedance increase and suppressing the continuous decomposition of the electrolyte.

SEM and TEM were used to obtain more insightful information on the morphology of the $LiNi_{0.5}Mn_{0.3}Co_{0.2}O_2$ cathode before and after cycling. Fig. 5 shows the surface morphology of the $LiNi_{0.5}Mn_{0.3}Co_{0.2}O_2$ electrodes before and after 100 cycles in various electrolytes. It was found that the $LiNi_{0.5}Mn_{0.3}Co_{0.2}O_2$ composite had spherical particles with a rough surface, composed of small primary crystals. However, morphology changes were observed for the electrodes after 100 cycles. As shown in Fig. 5b, the $LiNi_{0.5}Mn_{0.3}Co_{0.2}O_2$ composite cycled in EC-based electrolyte showed a smooth topography on the particle surface. The smooth surface was attributed to the consequent growth of SEI on the exposed surface of the $LiNi_{0.5}Mn_{0.3}Co_{0.2}O_2$ composite, accompanied by the decomposition of electrolyte at high voltage. For the electrode cycled in the FEC-based electrolyte (Fig. 5c), $LiNi_{0.5}Mn_{0.3}Co_{0.2}O_2$ particles together with carbon black were relatively uniformly dispersed in the matrix, and a small but detectable morphology change was found. In comparison, neither the obviously detectable morphology change nor the microstructural failure was observed for the $LiNi_{0.5}Mn_{0.3}Co_{0.2}O_2$ composite cycled in $LiPO_2F_2$-containing FEC-based electrolyte, even after 100 cycles (Fig. 5d). The thickness of the SEI films of the cycled cathodes in various electrolytes was characterized by TEM. The cathode cycled in the EC-based electrolyte was covered with a non-uniform and agglomerated SEI layer with a thickness of ~65 nm (Fig. 5e). With the addition of FEC, a slightly thinner SEI film (~45 nm) was formed on the cathode (Fig. 5f). As shown in Fig. 5g, significant improvements were observed for the cathode cycled in $LiPO_2F_2$-containing FEC-based electrolyte. The cathode was coated with a uniform and dense SEI film with a thickness of ~20 nm, which can ensure facile lithium-ion transport and mitigate the decomposition of the electrolyte. The SEI film formed in the $LiPO_2F_2$-containing FEC-based electrolyte was thinner and more stable than that of other electrolytes. Therefore, both FEC and $LiPO_2F_2$ should be responsible for the formation of a stable/durable SEI film that can protect the $LiNi_{0.5}Mn_{0.3}Co_{0.2}O_2$ cathode from the erosion of electrolyte.

The chemical composition of the cathode surface was studied by X-ray photoelectron spectroscopy (XPS), as shown in Fig. 6. For the C 1s spectra, three peaks were observed for the fresh electrode, C–C (284.8 eV), C–O (286.1 eV) and C–F (290.6 eV), corresponding to conductive carbon, polyether carbon $(-CH_2CH_2O-)_n$ and PVDF binder.[40,41] After cycling in EC-based electrolyte, the peak for C–F tended to be small, accompanied by the appearance of two new peaks of C=O (288.5 eV) and Li_2CO_3 (289.9 eV). These two peaks were caused by the decomposition of electrolyte during long-term cycling under high voltage.[42] However, the Li_2CO_3 peak disappeared and the C=O peak weakened for the electrode cycled in FEC-based electrolytes, which suggested that FEC-based electrolytes decomposed less than EC-based electrolytes at high voltages.[43] Combined with SEM, TEM, EIS and XPS results, the presence of many decomposition segments such as carbonyl groups can hardly protect the $LiNi_{0.5}Mn_{0.3}Co_{0.2}O_2$ cathode from sustained electrochemical side reactions with the electrolyte. Meanwhile, the thicker SEI layer generated in the EC-based electrolyte seemed to be difficult for Li^+ migration.

Besides the carbonyl-based organic components, inorganic species also played a crucial role to stabilize the SEI film on the cathode. For the F 1s spectra, the fresh electrode showed the C–F (687.7 eV) peak of PVDF, and this C–F peak was found to be smaller after cycling in the EC-based electrolyte, followed by a small LiF peak (684.8 eV).[44] It is well known that LiF is important to form a stable SEI film;[19] thus, a SEI formed on the cathode surface in EC-based electrolyte should not be stable. Compared with the EC-based electrolyte, the intensities of both C–F and LiF peaks tended to be larger after cycling in the FEC-based electrolyte. Therefore, in FEC-containing solutions, the SEI on the cathode was enriched with FEC and salt-reduction products, especially for LiF.[45] This composition of the surface film ensured long-term stable cycling of the battery in the FEC-based electrolyte. However, LiF has a lower conductivity, and the increase in LiF will result in weak Li^+ transmission, which is consistent with the results of the EIS spectra. The excessive LiF was derived from the hydrolysis of $LiPF_6$ ($LiPF_6 + H_2O \rightarrow POF_3 + HF + LiF$)[46,47] and the defluorination and ring opening of FEC by PF_5.[45,48,49] In constrast, the LiF peak significantly decreased for the electrode cycled in the $LiPO_2F_2$-containing FEC-based electrolyte. It was supposed that $LiPO_2F_2$ suppressed the hydrolysis of $LiPF_6$ and the side reaction between FEC and PF_5 produced by $LiPF_6$;[44,50,51] thus, the amount of LiF can be controlled within a reasonable range,[25] which not only reduced the electrochemical impedance of the SEI layer, but also ensured the cycling performance under high voltage.

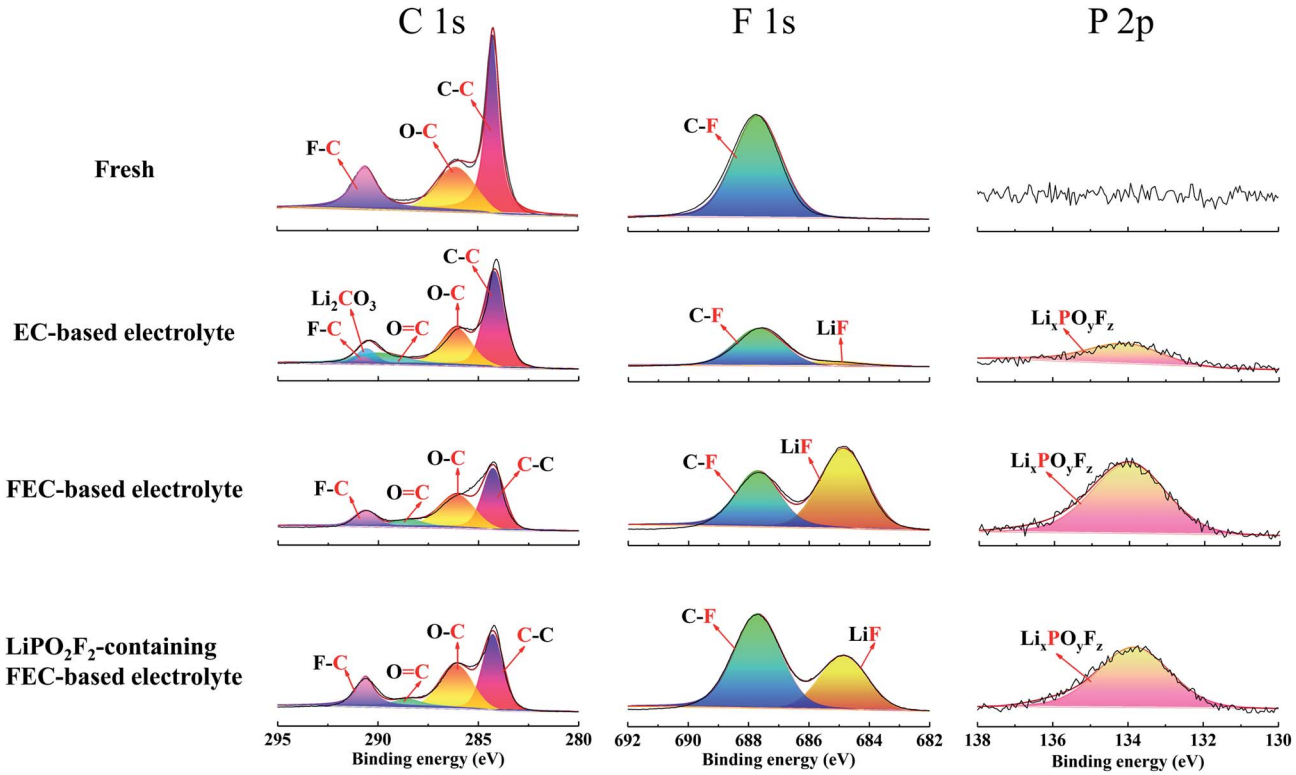

Fig. 6 The C 1s, F 1s, and P 2p spectra of the $LiNi_{0.5}Mn_{0.3}Co_{0.2}O_2$ cathodes using various electrolytes obtained after 50 cycles. The XPS spectra of the pristine $LiNi_{0.5}Mn_{0.3}Co_{0.2}O_2$ cathode are compared.

For the P 2p spectra, the EC-based electrolyte exhibited a small $Li_xPO_yF_z$ peak, which originated from the decomposition of $LiPF_6$ during cycling. The FEC-based electrolyte without $LiPO_2F_2$ showed the highest $Li_xPO_yF_z$ peak, because of the decomposition of $LiPF_6$ and the ring-opening reaction of FEC. However, the $Li_xPO_yF_z$ peak became smaller after the addition of $LiPO_2F_2$ in the FEC-based electrolyte. Therefore, the decomposition of $LiPF_6$ and the ring-opening reaction of FEC can be effectively inhibited by $LiPO_2F_2$, which agreed with the former result of the F 1s spectra.

To clarify the suppression of side reactions between FEC and products generated by $LiPF_6$, FEC-based electrolytes with and without $LiPO_2F_2$ were stored for several days, respectively. Deionized water (300 ppm) was added to each electrolyte sample before and after introducing $LiPO_2F_2$ into the electrolyte to confirm the reactivity of $LiPO_2F_2$ toward the products of $LiPF_6$. The changes in the color and pH before and after storage at room temperature for three days are shown in Fig. 7. Before storage, the appearances of the electrolytes with and without $LiPO_2F_2$ were similar and the electrolytes were transparent. However, the color of the electrolyte without $LiPO_2F_2$ changed from colorless to brown after storage, while almost no change happened for the electrolyte with $LiPO_2F_2$. In addition, the pH paper dipped in the electrolyte without $LiPO_2F_2$ became red, indicating a strong acid. In contrast, a slight color change was observed for the pH paper dipped in the electrolyte with $LiPO_2F_2$. As previously reported,[46,47] this was ascribed to the hydrolysis reaction of $LiPF_6$ to form PF_5, HF, and POF_3, which can react with the FEC solvent to form a colored substance. By adding the $LiPO_2F_2$, the hydrolysis of $LiPF_6$ can be suppressed due to the higher promoters of ion-paired $LiPF_6$ dissociation,[26,47] resulting in the great stability and ionic conductivity of

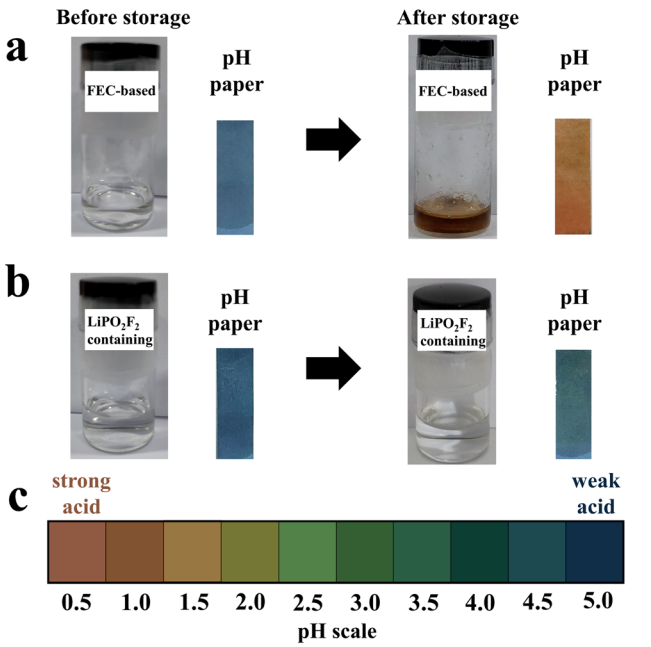

Fig. 7 Photographs of the solvent mixtures: (a) FEC-based electrolyte with 300 ppm H_2O before and after storage for 3 days. (b) $LiPO_2F_2$-containing FEC-based electrolyte with 300 ppm H_2O before and after storage for 3 days. (c) Indicator chart for the pH scale.

the electrolyte. Moreover, the $PO_2F_2^-$ as a reaction product may have inhibited the progress of the reaction ($POF_3 + H_2O \rightarrow PO_2F_2^- + H^+ + HF$).

4. Conclusion

The electrochemical properties of $LiNi_{0.5}Mn_{0.3}Co_{0.2}O_2$ were investigated under high voltage in EC-based, FEC-based and $LiPO_2F_2$-containing FEC-based electrolytes, respectively. The $LiNi_{0.5}Mn_{0.3}Co_{0.2}O_2$ in $LiPO_2F_2$-containing FEC-based electrolyte exhibited excellent cycling stability with a reversible capacity of 157.7 mA h g^{-1} over 200 cycles at 1C rate. The morphology and component analysis of the SEI film on the cathode were characterized by SEM, TEM and XPS, respectively. Based on SEM, TEM and XPS results, the component of SEI was optimized by using the FEC and $LiPO_2F_2$ to form a thin and stable SEI layer, which dramatically suppressed the decomposition of the electrolyte. Furthermore, the SEI layer formed in $LiPO_2F_2$-containing FEC-based electrolyte had great ionic conductivity, resulting in a significant improvement of the electrochemical performances, including enhanced capacity retention, and superior rate capability. $LiPO_2F_2$ can also effectively suppress the side reaction between FEC and products generated by $LiPF_6$ in the electrolyte. These findings will encourage more empirical investigations into the synergistic effect between cosolvents and additives for Li-ion batteries.

Conflicts of interest

There are no conflicts to declare.

Acknowledgements

This work was financially supported by the National Natural Science Foundation of China (21606135), the Science Technology Innovation Research Program of Ningbo (2019B10113). This work was also sponsored by K. C. Wong Magna Fund in Ningbo University.

References

1 A. Kraytsberg and Y. Ein-Eli, *Adv. Energy Mater.*, 2012, **2**, 922–939.
2 M. S. Whittingham, *Chem. Rev.*, 2004, **104**, 4271–4301.
3 M. M. Thackeray, S.-H. Kang, C. S. Johnson, J. T. Vaughey, R. Benedek and S. A. Hackney, *J. Mater. Chem.*, 2007, **17**, 3112–3125.
4 Z. Lu, D. D. MacNeil and J. R. Dahn, *Electrochem. Solid-State Lett.*, 2001, **4**, A191–A194.
5 L. Yang, B. Ravdel and B. L. Lucht, *Electrochem. Solid-State Lett.*, 2010, **13**, A95–A97.
6 K. Xu, *Chem. Rev.*, 2014, **114**, 11503–11618.
7 L. Hu, Z. Zhang and K. Amine, *J. Power Sources*, 2013, **236**, 175–180.
8 D. Lu, M. Xu, L. Zhou, A. Garsuch and B. L. Lucht, *J. Electrochem. Soc.*, 2013, **160**, A3138–A3143.
9 A. Ramasubramanian, V. Yurkiv, T. Foroozan, M. Ragone, R. Shahbazian-Yassar and F. Mashayek, *J. Phys. Chem. C*, 2019, **123**, 10237–10245.
10 S. J. Park, J. Y. Hwang, C. S. Yoon, H. G. Jung and Y. K. Sun, *ACS Appl. Mater. Interfaces*, 2018, **10**, 17985–17993.
11 J. M. Tarascon, C. Delacourt, A. S. Prakash, M. Morcrette, M. S. Hegde, C. Wurm and C. Masquelier, *Dalton Trans.*, 2004, **19**, 2988–2994.
12 T. Achiha, T. Nakajima, Y. Ohzawa, M. Koh, A. Yamauchi, M. Kagawa and H. Aoyama, *J. Electrochem. Soc.*, 2010, **157**, A707–A712.
13 M. Hu, X. Pang and Z. Zhou, *J. Power Sources*, 2013, **237**, 229–242.
14 Z. Zhang, L. Hu, H. Wu, W. Weng, M. Koh, P. C. Redfern, L. A. Curtiss and K. Amine, *Energy Environ. Sci.*, 2013, **6**, 1806–1810.
15 A. O. Kondrakov, H. Geßwein, K. Galdina, L. de Biasi, V. Meded, E. O. Filatova, G. Schumacher, W. Wenzel, P. Hartmann, T. Brezesinski and J. Janek, *J. Phys. Chem. C*, 2017, **121**, 24381–24388.
16 T. Li, X. Q. Zhang, P. Shi and Q. Zhang, *Joule*, 2019, **3**, 2647–2661.
17 P. Verma, P. Maire and P. Novák, *Electrochim. Acta*, 2010, **55**, 6332–6341.
18 M. He, L. Hu, Z. Xue, C. C. Su, P. Redfern, L. A. Curtiss, B. Polzin, A. von Cresce, K. Xu and Z. Zhang, *J. Electrochem. Soc.*, 2015, **162**, A1725–A1729.
19 E. Markevich, G. Salitra, F. Chesneau, M. Schmidt and D. Aurbach, *ACS Energy Lett.*, 2017, **2**, 1321–1326.
20 G. Salitra, E. Markevich, M. Afri, Y. Talyosef, P. Hartmann, J. Kulisch, Y. K. Sun and D. Aurbach, *ACS Appl. Mater. Interfaces*, 2018, **10**, 19773–19782.
21 X. Fan, L. Chen, O. Borodin, X. Ji, J. Chen, S. Hou, T. Deng, J. Zheng, C. Yang, S. C. Liou, K. Amine, K. Xu and C. Wang, *Nat. Nanotechnol.*, 2018, **13**, 715–722.
22 Y. Li, Y. Li, A. Pei, K. Yan, Y. Sun, C. L. Wu, L. M. Joubert, R. Chin, A. L. Koh, Y. Yu, J. Perrino, B. Butz, S. Chu and Y. Cui, *Science*, 2017, **358**, 506–510.
23 Y. Li, W. Huang, Y. Li, A. Pei, D. T. Boyle and Y. Cui, *Joule*, 2018, **2**, 2167–2177.
24 K. E. Kim, J. Y. Jang, I. Park, M.-H. Woo, M.-H. Jeong, W. C. Shin, M. Ue and N.-S. Choi, *Electrochem. Commun.*, 2015, **61**, 121–124.
25 B. Yang, H. Zhang, L. Yu, W. Fan and D. Huang, *Electrochim. Acta*, 2016, **221**, 107–114.
26 W. Zhao, G. Zheng, M. Lin, W. Zhao, D. Li, X. Guan, Y. Ji, G. F. Ortiz and Y. Yang, *J. Power Sources*, 2018, **380**, 149–157.
27 S. Hong, B. Hong, W. Song, Z. Qin, B. Duan, Y. Lai and F. Jiang, *J. Electrochem. Soc.*, 2018, **165**, A368–A370.
28 C. Wang, L. Yu, W. Fan, R. Liu, J. Liu, L. Ouyang, L. Yang and M. Zhu, *J. Alloys Compd.*, 2018, **755**, 1–9.
29 G. Cherkashinin, M. Motzko, N. Schulz, T. Spath and W. Jaegermann, *Chem. Mater.*, 2015, **27**, 2875–2887.
30 B. J. Hwang, Y. W. Tsai, D. Carlier and G. Ceder, *Chem. Mater.*, 2003, **15**, 3676–3682.

31 D. Zhou, A. Tkacheva, X. Tang, B. Sun, D. Shanmukaraj, P. Li, F. Zhang, M. Armand and G. Wang, *Angew. Chem., Int. Ed.*, 2019, **58**, 6001–6006.
32 K. Karuppasamy, P. A. Reddy, G. Srinivas, A. Tewari, R. Sharma, X. S. Shajan and D. Gupta, *J. Membr. Sci.*, 2016, **514**, 350–357.
33 X. Pan, T. Liu, D. J. Kautz, L. Mu, C. Tian, T. E. Long, P. Yang and F. Lin, *J. Power Sources*, 2018, **403**, 127–136.
34 K. Karuppasamy, P. A. Reddy, G. Srinivas, R. Sharma, A. Tewari, G. H. Kumar and D. Gupta, *J. Solid State Electrochem.*, 2016, **21**, 1145–1155.
35 H.-B. Han, K. Liu, S. W. Feng, S.-S. Zhou, W.-F. Feng, J. Nie, H. Li, X.-J. Huang, H. Matsumoto, M. Armand and Z. B. Zhou, *Electrochim. Acta*, 2010, **55**, 7134–7144.
36 X. Sun, H. S. Lee, X. Q. Yang and J. McBreen, *Electrochem. Solid-State Lett.*, 2002, **5**, A248–A251.
37 H. Zhang, G. Cao, Y. Yang and Z. Gu, *J. Am. Chem. Soc.*, 2008, **46**, 30–34.
38 P. L. Taberna, P. Simon and J. F. Fauvarque, *J. Electrochem. Soc.*, 2003, **150**, A292–A300.
39 R. de Levie, *Electrochim. Acta*, 1963, **8**, 751–780.
40 R. Dedryvère, D. Foix, S. Franger, S. Patoux, L. Daniel and D. Gonbeau, *J. Phys. Chem. C*, 2010, **114**, 10999–11008.
41 H. Bouayad, Z. Wang, N. Dupré, R. Dedryvère, D. Foix, S. Franger, J. F. Martin, L. Boutafa, S. Patoux, D. Gonbeau and D. Guyomard, *J. Phys. Chem. C*, 2014, **118**, 4634–4648.
42 K. Ushirogata, K. Sodeyama, Y. Okuno and Y. Tateyama, *J. Am. Chem. Soc.*, 2013, **135**, 11967–11974.
43 G. Yan, X. Li, Z. Wang, H. Guo, W. Peng, Q. Hu and J. Wang, *J. Solid State Electrochem.*, 2017, **21**, 1589–1597.
44 J. Cha, J. G. Han, J. Hwang, J. Cho and N.-S. Choi, *J. Power Sources*, 2017, **357**, 97–106.
45 K. Kim, I. Park, S. Y. Ha, Y. Kim, M. H. Woo, M. H. Jeong, W. C. Shin, M. Ue, S. Y. Hong and N.-S. Choi, *Electrochim. Acta*, 2017, **225**, 358–368.
46 L. Q. Zheng, S. J. Li, H. J. Lin, Y. Y. Miao, L. Zhu and Z. J. Zhang, *Russ. J. Electrochem.*, 2014, **50**, 904–907.
47 J. G. Han, K. Kim, Y. Lee and N. S. Choi, *Adv. Mater.*, 2019, **31**, 1804822.
48 C. Xu, F. Lindgren, B. Philippe, M. Gorgoi, F. Björefors, K. Edström and T. Gustafsson, *Chem. Mater.*, 2015, **27**, 2591–2599.
49 X. Chen, X. Li, D. Mei, J. Feng, M. Y. Hu, J. Hu, M. Engelhard, J. Zheng, W. Xu, J. Xiao, J. Liu and J. G. Zhang, *ChemSusChem*, 2014, **7**, 549–554.
50 C. K. Kim, D. S. Shin, K. E. Kim, K. Shin, J. J. Woo, S. Kim, S. Y. Hong and N.-S. Choi, *ChemElectroChem*, 2016, **3**, 913–921.
51 G. Yang, J. Shi, C. Shen, S. Wang, L. Xia, H. Hu, H. Luo, Y. Xia and Z. Liu, *RSC Adv.*, 2017, **7**, 26052–26059.